Proceedings of the Federated Conference on
Computer Science and Information Systems pp. 255–260

ISBN 978-83-60810-22-4

Numerical Assessment of Finite Difference Time Domain and Complex-Envelope Alternating-Direction-Implicit Finite-Difference-Time-Domain Methods

Gebriel A. Gannat
Engineering Department
Sharjah Colleges, HCT, UAE
P.O.Box 7947
E-mail ggannat@hct.ac.ae

***Abstract*—A thorough numerical assessment of Finite Difference Time Domain and Complex-Envelope Alternating-Direction-Implicit Finite-Difference-Time-Domain Methods has been carried out based on a basic single mode Plane Optical Waveguide structure. Simulation parameters for both methods were varied and the impact on the performance of both numerical methods is investigated.**

I. Introduction

DIFFERENT numerical modelling techniques have been proposed in literature to analyse optical and photonic devices, such as Beam Propagation method (BPM) [1], Finite-Element-Time-Domain (FETD) method [2] and Finite-Difference-Time-Domain [3] method. The Finite Difference Time Domain (FDTD) is a very popular method mainly because of its ability to simulate ultra-complicated structures in a very simple and straightforward manner. However, as main drawback, FDTD requires high computational resources due to Courant criterion which limits the time step size in order to preserve the numerical stability of the scheme. As an efficient alternative to FDTD, Complex-Envelope Alternating-Direction-Implicit Finite-Difference-Time-Domain (CE-ADI-_FDTD) method [4] has been proposed in literature. The main advantage of CE-ADI-FDTD is the time step sizes not bounded by the Courant criterion making virtually possible to employ larger time step sizes with low impact on accuracy and great saving in terms of computational resources. But the approach proposed in [4] has been proven to suffer from numerical instability due to the Absorbing Boundary Conditions (ABCs) [4]-[7]. This instability affects the maximum time step size that is possible to use in order to maintain the scheme stable limiting the numerical efficiency of the method itself. In [5], an improved formulation of the ABCs has been implemented in the context of CE-ADI-FDTD making the numerical scheme stable even for very large time step sizes. The focus in this paper is to assess and investigate the performance of FDTD and CE-ADI-FDTD methods against Courant, Friederich, Levy Criterion (CFL) and different parameters of Uniaxial Perfectly Matched Layer (UPML). Parameters such as geometric coefficient (g), number and size of PML cells were varied for a number of simulations and the obtained results are presented in this paper.

II. ASSESSMENT OF FDTD METHOD

A simple waveguide structure shown in Fig .1 is simulated using the developed FDTD code to investigate the performance of the FDTD method. As shown in this figure, the refractive indices of the core and cladding are 3.2 and 1, respectively. The structure is discretised into a uniform mesh and is terminated by 20 cells UPML to absorb the reflected power. To ensure the single mode propagation at 1.55μm wavelength, the width (W) of the waveguide chosen to be 0.2μm. All the results for the reflected power are obtained by injecting a source-field along the transverse x direction, modulated at wavelength 1.55μm and 5-fs wide Gaussian pulse. The source-fields for TE and TM used is presented by the equations given below;

$$E_{z_{i,j}}^{n+1} = E_{z_{i,j}}^{n} \phi_j \sin\left(2\pi\, fn\, \Delta t\right) e^{\left((n\Delta t - 3\mathrm{T})/T\right)^2} \quad (1a)$$

$$H_{z_{i,j}}^{n+1} = H_{z_{i,j}}^{n} \phi_j \sin\left(2\pi\, fn\, \Delta t\right) e^{\left((n\Delta t - 3\mathrm{T})/T\right)^2} \quad (1b)$$

As shown in Fig. 1, the detector point is labelled as D1 to record the incident and the reflected power inside the waveguide. Once the incident and reflected power recorded in D1, the ratio of FFT of the reflected to incident field is calculated to compute the spectrum variation of the reflected power coefficient.

As shown in Fig. 1, the reference point is labelled as D1 to record the incident field transmitted and reflected power from the PML inside the waveguide, respectively. Once the transmitted power reaches the output terminal of the waveguide, the ratio of FFT of the reflected to incident field is calculated to compute the spectrum variation of the reflected power coefficient.

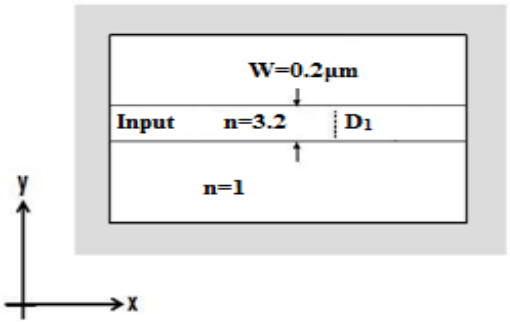

Fig. 1 Basic single mode waveguide, width (W) = 0.2μm and refractive index, n= 3.2

A. *Assessment of FDTD against Courant, Friederich, Levy Criterion (CFL)*

In order to investigate the effect of CFL criterion on the performance of the FDTD, the waveguide structure, shown in Fig. 1 is simulated using the developed FDTD code. The TE-mode and TM-mode source field given by equations (1a) and (1b) are injected inside the waveguide along the transverse x direction [8], modulated at wavelength 1.55μm and 5-*fs* wide. At the first simulation Δt chosen to be larger than the CFL criterion and the structure is discretised into a uniform mesh with cell size of 20nm. Δt used in the simulation can be calculated as follows;

$$\Delta t > \frac{1}{c\sqrt{\frac{1}{(\Delta x)^2}+\frac{1}{(\Delta y)^2}}} \qquad (2)$$

Based on the parameters stated above, field profile shown in Fig. 2 is obtained. As it may be observed from the Figure, the field profile inside the waveguide is instable and constantly increases as the time step increases. As a result of this stability problem, the propagation of the field profile inside the waveguide can not be simulated. The FDTD code has been tested when Δt> $2*(\Delta t)_{CFL}$, and Δt> $3*(\Delta t)_{CFL}$ and it has been observed that field profile is extremely instable when CFL criterion not applied. On other words FDTD is absolutely useless to simulate wave propagation if CFL criterion is not applied.

The simulation parameters modified and Δt chosen to be less than $(\Delta t)_{CFL}$ and the obtained result is presented in Fig. 3. As it may observed that the field profile presented in Fig. 3 represents a Gaussian pulse which is given by the equation (1) and therefore a stable field profile will propagate inside the waveguide and the transmitted and reflected power can be observed along the waveguide.

B. *Assessment of UPML Reflection.*

For further assessment of the FDTD scheme, the reflected power coefficient of the UPML is investigated for both TE-mode and TM mode. In order to investigate

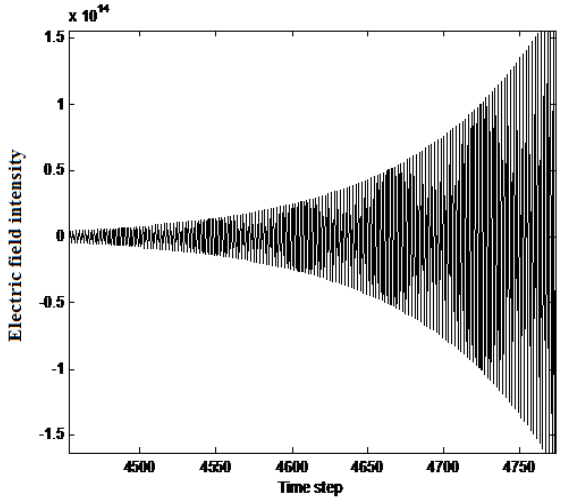

Fig. 2: Time variation of the electric field recorded at point detector D1 inside the waveguide presented in Fig. 1,when

$$\Delta t > (\Delta t)_{CFL}$$

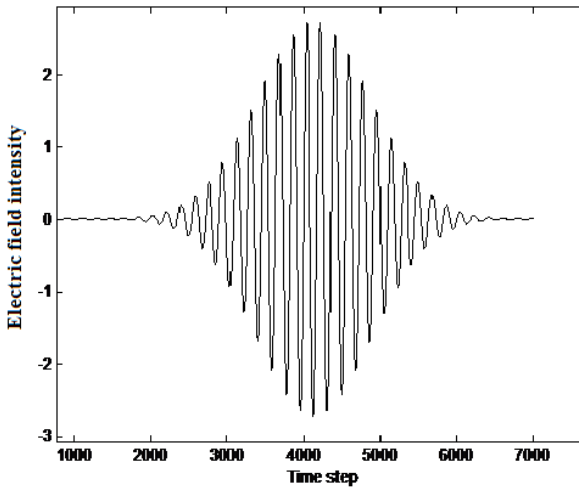

Fig. 3 Time variation of the electric field recorded at point detector D1 inside the waveguide presented in Fig. 1, when

$$\Delta t < (\Delta t)_{CFL}$$

the effect of the scaling factor (g) on the reflected power coefficient, the structure presented in Fig.1 is simulated for three different values of scaling factor ***(g)*** for both TE and TM mode of propagation. The central wavelength, λ is 1.55μm, the size of discretisation cell (Δx and Δy) are 30nm, and the number of UPML cells is 20 .

As it may be observed from Fig. 4a, the reflected power coefficient for TE-mode is obtained for a different scaling factor, *g*=1.5, 2.5 and 3.5. The reflected power coefficients obtained are about -37dB, -25dB and -19 dB, respectively. From the obtained results, it can be observed that minimum reflected power coefficient is obtained when g is equal to 1.5 and therefore this figure is considered for the rest of the simulations in this research study.

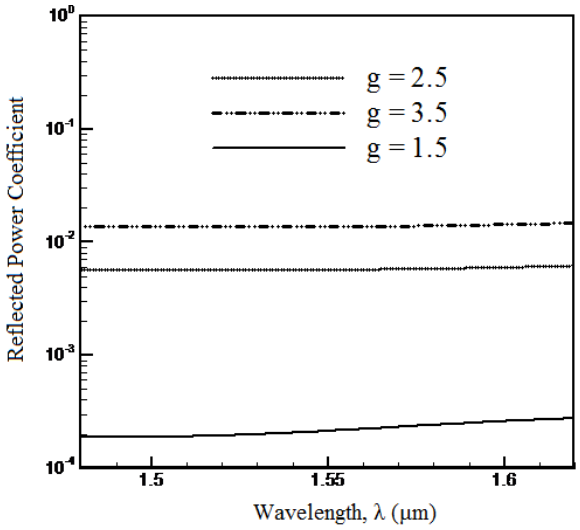

Fig. 4a: Variation of UPML reflected power coefficient for TE-Mode against the wavelength for three different values of *"g"* at central wavelength 1.55μm.

Similarly, the reflected power coefficients for TM-mode are obtained for the same values of *(g)* and as presented in Fig. 4b, the values of the reflected power coefficients obtained for TM-mode are about -40dB, -30dB and -27dB respectively. From both figures it can be observed that the reflected power coefficient for both propagation modes (TE and TM) is very low and the UPML gives a higher performance when the scaling factor *(g)* chosen around 1.5 and therefore this figure is considered for the rest of the simulations.

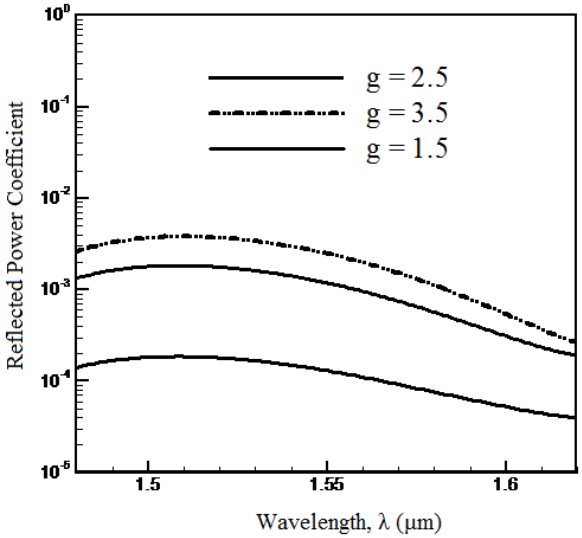

Fig. 4b: Variation of UPML reflected power coefficient for TM-Mode against the wavelength for three different values of "*g*" at central wavelength 1.55μm.

For further assessments of the reflected power coefficient of UPML for both TE and TM mode of propagation, the structure presented in Fig. 1 is simulated for 10, 20, 30 and 40 UPML cells. The central wavelength, λ is 1.55μm, the size of discretisation cell (Δx = Δy=30nm), and the scaling factor (g) is 1.5. As it may observed from Fig. 5a, the lowest reflected power coefficient or TE-mode is obtained when number of UPML cells used is 20, 30 and 40. The reflected power coefficient obtained is about (-38dB). The highest reflected power coefficient is obtained when 10 UPML cells are used and the obtained is about (-20dB).

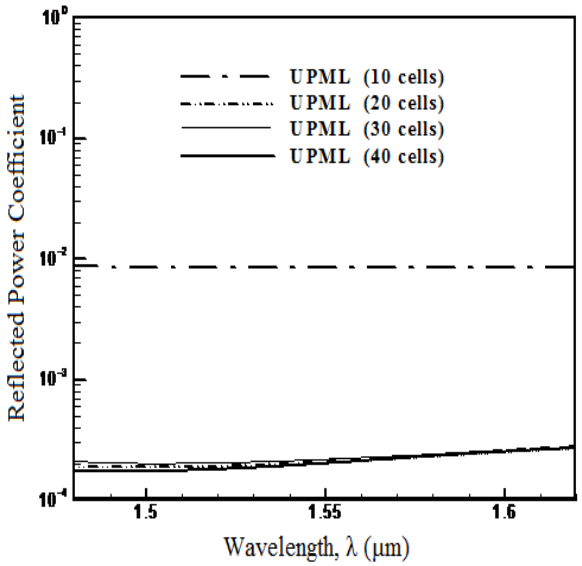

Fig. 5a: Variation of UPML reflected power coefficient of TE-Mode against wavelength, λ when the number of UPML cells is a parameter

When the number of UPML cells increased the UPML layers thickness increases and the ability to absorb incident power on the boundaries increases, this improves the performance of the UPML layer and minimise the reflected power from the UPML boundaries. Similarly, the reflected power coefficients for TM-mode are obtained for the same numbers of UPML cells. As presented in Fig. 5b, the values of the reflected power coefficient are slightly different from TE-mode. When the number of UPML cells used is 20, 30 and 40 reflected power coefficient is slightly below (-40db) and when UPML cells chosen to be 10, the reflected power coefficient obtained about (-35dB). Overall the reflection ratios for both TE and TM propagation mode are very low and this will help the accuracy of the results obtained by the simulations in more complex structures.

For further investigation the structure presented in Fig. 1 is simulated using different sizes of discretisation cell (Δx = Δy) at central wavelength, λ is 1.55μm and the scaling factor, *g* is 1.5. As it may be observed from Fig. 6a, *Δx* and *Δy* values used in the simulations are 10, 20 and 30 nm and the obtained reflected power coefficients are -28dB, -35dB and -39dB respectively. Experimentally Δ*x* and Δy need to < 0.05*a*. Generally, for the TE-mode the reflected power coefficients for the three different values of *Δx* and *Δy* are very low. However it can be concluded that the reflected power coefficients are inverse proportional to the size of the discreti-

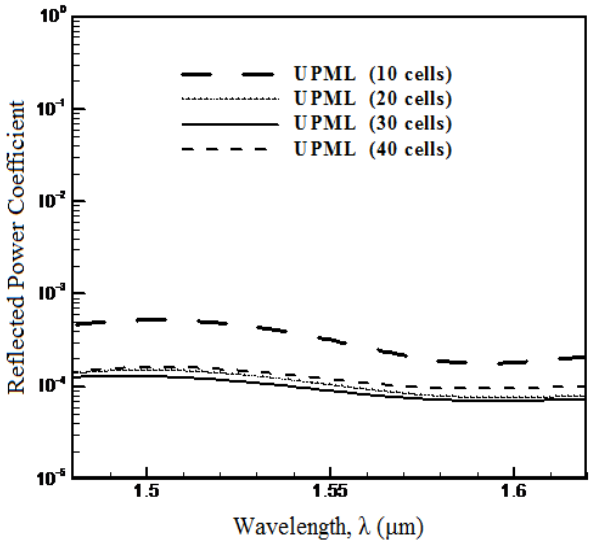

Fig. 5b: Variation of UPML reflected power coefficient for TM-Mode against the wavelength, λ when the number of UPML cells is a parameter.

sation cell, in other words the larger the cell the lowest the reflected power coefficients.

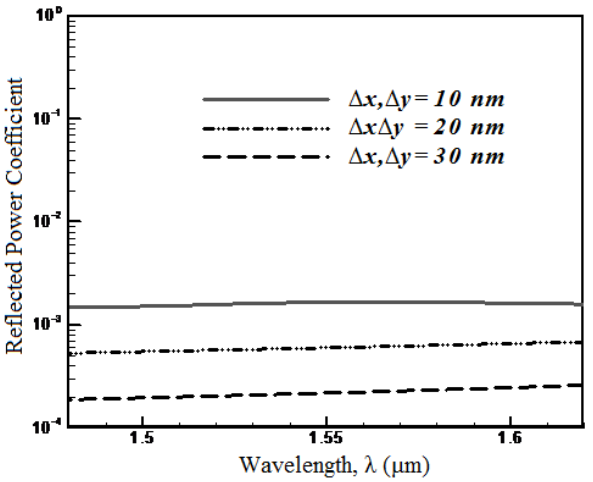

Fig. 6a: Variations of UPML reflected power coefficient of TE-Mode against wavelength, λ when Δx and Δy size is a parameter.

Fig. 6b presents the variation of reflected power coefficient with the wavelength for different values of discretisation cells. As it may observed from the graphs, when Δx and Δy value is 10 nm, the reflected power coefficient reaches the lowest value (-40dB) at the central wavelength, λ is 1.55μm, when Δx and Δy value is 30 nm, the reflected power coefficient at the central wavelength is about - reflected power coefficient 40dB, however it reaches the lowest value (-50dB) at the wavelength, λ is 1.55μm. Meanwhile, when Δx and Δy value is 20 nm, the is about -36dB and similar cross the bandwidth.

III. Assessment of CE-ADI-FDTD Method.

The same waveguide structure presented in Fig. 1 is simulated using the developed CE-ADI-FDTD code to

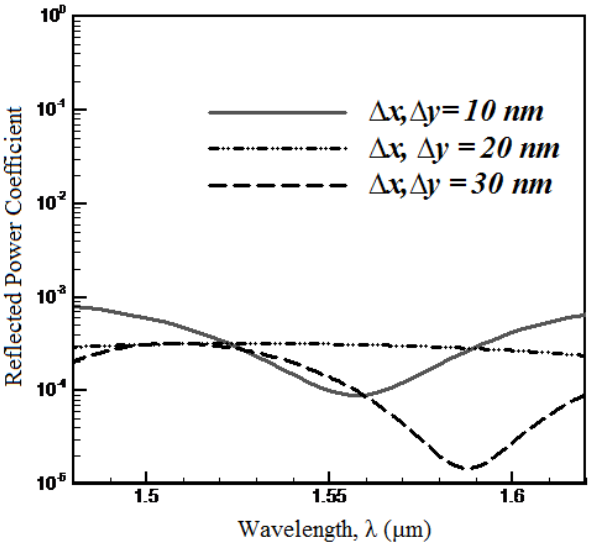

Fig. 6b: Variations of UPML reflected power coefficient of TM-Mode against the wavelength, λ when Δx and Δy size is a parameter.

investigate the performance of the CE-ADI-FDTD method. As shown in this figure, the refractive indices of the core and cladding are 3.2 and 1, respectively. The structure is discretised into a uniform mesh and is terminated by 20 cells PML to absorb the reflected power. To ensure the single mode propagation at 1.55μm wavelength, the width of the waveguide is chosen to be 0.2μm.

A. Assessment of CE-ADI-FDTD against CFL Criterion.

In order to investigate the effect of CFL criterion on the performance of the CE-ADI-FDTD, the waveguide structure presented in Fig. 1 is simulated using the developed FDTD code. The TE-mode source-field given by equation (1a) injected inside the waveguide along the transverse *x* direction, modulated at wavelength 1.55μm and 5-fs wide. The structure is discretised into a uniform mesh with cell size of 20nm.

For the first simulation, Δt chosen to be ten times larger than the CFL criterion, ($\Delta t = 10(\Delta t)_{CFL}$) and the structure is discretised into a uniform mesh with cell size of 20nm. Based on the parameters stated above the CE-ADI-FDTD tested for ($\Delta t = 10(\Delta t)_{CFL}$) and ($\Delta t = 30(\Delta t)_{CFL}$) and the field profile shown in Fig. 7 is obtained. As it may be observed from the Figure, the field profile inside the waveguide is very stable and the CFL criterion is completely eliminated. Furthermore the same structure simulated with Δt chosen to be less than the CFL criterion, ($\Delta t = 0.9(\Delta t)_{CFL}$) and the obtained field profile shown in Fig. 8 is very stable.

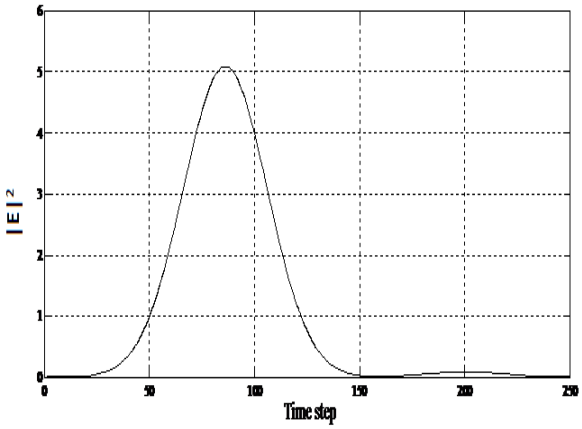

Fig. 7: Time variation of the envelopes of the electric field recorded at point detector D1 inside the waveguide presented in Fig. 1, when $\Delta t > (\Delta t)_{CFL}$

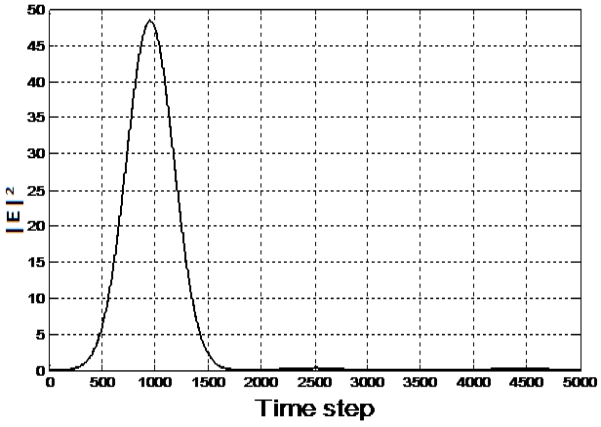

Fig. 8: Time variation of the envelopes of the electric field recorded at point detector D1 inside the waveguide presented in Fig. 1, when $\Delta t < (\Delta t)_{CFL}$

B. Assessment of PML Reflection

For further assessment of the CE-ADI-FDTD scheme, the reflected power coefficient of the PML is investigated for TE-mode. In order to investigate the effect of the scaling factor *(g)* on the reflected power coefficient, the structure presented in Fig. 1 is simulated for three different values of scaling factor *(g)*. The central wavelength, λ is 1.55μm, the size of discretisation cell, Δx and Δy is 30nm, and the number of PML cells is 20 . As it may be observed from Fig. 9, that the lowest reflected power coefficient obtained when the scaling factor (g) is equal to 1.5, it is about (-50dB).

In order to investigate the effect of time step (Δt) on the reflected power coefficient, the structure presented in Fig. 1 simulated for three different values of Δt. The central wavelength, λ is 1.55 μm, the size of discretisation cell, Δx and Δy is 30nm, and the number of PML cells is =20 . It may observed form Fig. 10 the reflected power coefficients obtained for three different values of Δt are about the same and therefore it may be concluded that using a large Δt value it will have no major impact on the accuracy of the CE-ADI-FDTD scheme.

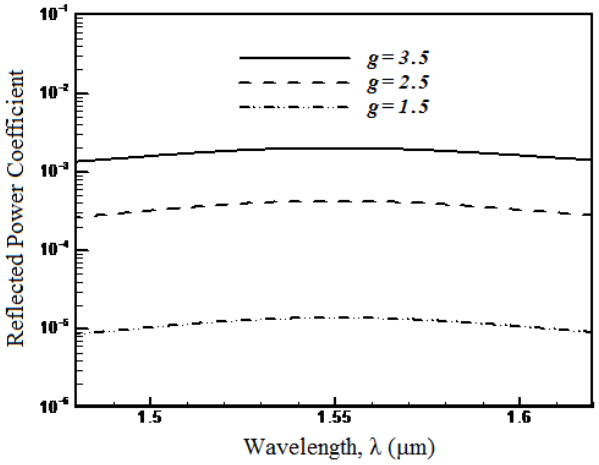

Fig. 9: Variations of PML reflected power coefficient of TE-Mode against the wavelength for three different values of "g" at central wavelength 1.55μm.

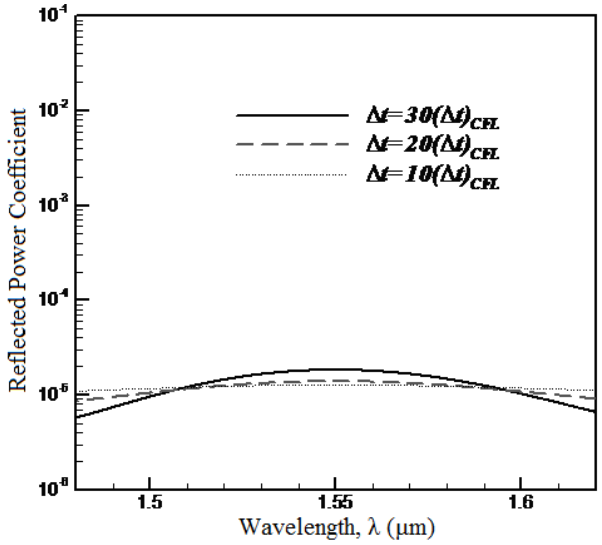

Fig. 10: Variations of PML reflected power coefficients with the wavelength for different values of Δt at central wavelength 1.55μm.

Furthermore, the same structure presented in Fig. 1 is simulated to investigate the effect of the size of the discretisation cells on the reflected power coefficient. Discretisation cells in x and y direction are chosen to be equal and the structure simulated three times using cell size 10, 20 and 30nm. As it may observed from Fig. 11, the lowest value of reflected power coefficient obtained is about -55dB when the cell size is 20nm.

IV. Conclusion

In this paper a number of simulations have been carried out in order to investigate the performance of the FDTD and CE-ADI-FDTD for different simulation parameters such as, Courant, Friederich, Levy Criterion, scaling factor (g), size and number of discretisation cells. From the simulation results presented can be observed that the applying of Courant, Friederich, Levy

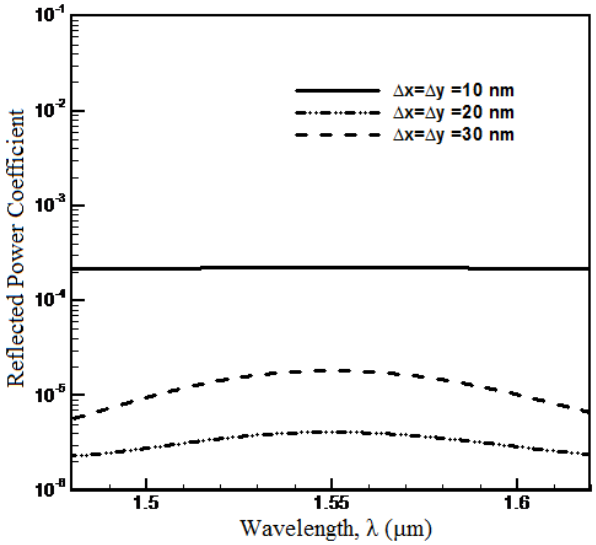

Fig. 11: Variations of PML reflected power coefficients with the wavelength for different values of *Δx, Δy* at central wavelength 1.55μm

Criterion has a big impact on the stability of the simulation in FDTD method but has no impact on CE-ADI-FDTD in terms of stability. The scaling factor (g), cell size and thickness of PML layer have an impact on the reflected power coefficient for both FDTD and CE-ADI-FDTD and have to be selected carefully.

References

[1] Patrocínio da Silva J., Hernández-Figueroa H. E., and Ferreira Frasson A. M., "Improved Vectorial Finite-Element BPM Analysis for Transverse Anisotropic Media," *IEEE J. Lightwave Technol.,* 2003, 21, (2), pp. 567-576.

[2] S. S. A. Obayya, B. M. Rahman, and H. A. El-Mikati, "New Full Numerical Efficient Propagation Algorithm Based on the Finite Element Method," *IEEE J. Quantum Electron.,* vol. 18, no. 3, pp. 409-415, March 2000.

[3] M. De Pourcq, and C. Eng, "Field and Power-Density Calculations in Closed Microwave Systems by Three- Dimensional Finite Difference", *IEE Proc. H Microwaves, Antennas & Propagation*, Vol. 132, pp. 360-368, Oct. 1985.

[4] Rao H., Scarmozzino R., and Osgood R. M.: 'An Improved ADI-FDTD Method and Its Application to Photonic Simulations', IEEE Photon. Technol. Lett., 2002, 14, (4), pp. 477-479.

[5] Pinto D., and Obayya S. S. A.: 'Improved Complex-Envelope Alternating-Direction-Implicit Finite-Difference-Time-Domain Method for Photonic-Bandgap Cavities', IEEE J. Lightwave Technol., 2007, 25, (1), pp. 440-447.

[6] T. Namiki, and K. Ito, "Investigation of Numerical Errors of The Two-Dimensional ADI-FDTD Method," *IEEE Trans. Microw. Theory Tech.*, Vol. 48, no. 11, pp. 1950 – 1956, Nov. 2000.

[7] Sai-tak Chu and Sujeet K. Chaudhuri "A Finite-Difference Time-Domain Method for the Design and Analysis of Guided-Wave Optical Structure," *J. Lightwave Technol*., vol. 7, no.12, pp. 2033-2038, Dec. 1989.

[8] A. Taflove, *Computational Electrdynamics*: *The finite Difference Time Domain Method*. Boston, MA: Artech, 1995